DFT and TD-DFT Studies of 1,3,5-Tris (Dipheny1amino) Benzene Derivatives Based Hole Transport Materials: Application for Perovskite Solar Cells

nambury surendra babu (nsbabusk@gmail.com)
The university of Dodoma https://orcid.org/0000-0003-3851-9361
Irene Octavian Riwa
The University of Dodoma College of Natural Sciences and Mathematics

Research Article

Keywords: Perovskite Solar cells, hole transport materials, DFT method, photoelectric properties and reorganization energies.

Posted Date: January 12th, 2022

DOI: https://doi.org/10.21203/rs.3.rs-1041718/v1

Abstract

The current study examined a series of 1,3,5-tris (diphenylamino) benzene derivatives used as hole transport materials in perovskite solar cells (HTM1-HTM9). DFT and TD/DFT with the B3LYP/6-311G basis set used for all calculations. The ground state geometry, frontier molecular orbital (FMO), photoelectric properties and reorganization energies and the absorption spectra were investigated. The energy levels of HOMO and LUMO orbitals were calculated for HTM1-HTM9, compared to all of the compounds under investigation and the spiro-OMeTAD, HTM 8 has the lowest HOMO energy level, indicating a favourable overlap with the MAPbI3 perovskite active layer.

1. Introduction

Perovskite solar cells (PSCs) have significant attention for academia and industry, Due to outstanding qualities such as efficiency, low cost, and simple assembly using roll-to-roll processing [1–3]. In photovoltaics, perovskite materials are game-changers. The performance of perovskite solar cells has recently increased from 3.7 % to 25.2 % in a brief period, making it a formidable competitor to silicon solar cells [4]. A light-absorbing layer is commonly placed between the electron transport material (ETM) and PSCs' hole transport material (HTM). At the interface between the HTM and the perovskite layer, the HTM's role is to allow hole extraction while preventing charge recombination. To justify their use, suitable materials should have tremendous hole transport capacity and conductivity, high mobility [5]. In addition, the HOMO orbital energy level should be well aligned with the valence band of the perovskite material [6] and good solubility to aid processability, and low cost [7].

The efficiency of a solar device is determined mainly by charge generation and passage to the appropriate electrodes. After the electrons/holes are generated and transferred to their charge transport layers, they are collected at their corresponding electrodes, resulting in a photocurrent. Solar cells are also subject to undesired processes, such as recombining charged species, which reduces efficiency [8]. The charge generation, separation, and extraction processes must occur faster than the recombination process to achieve high efficiency. Charges (holes/electrons) are better extracted and transported from the absorbing layer to the electrodes when interfacial layers are present; they also prevent the flow of oppositely charged ions.

HTMs are critical to device performance because they: i) change the energy barrier height between an electrode and the active layer; ii) form a specific contact for carriers; iii) protect a physical and chemical reaction between the electrode and the active layer; iv) aid in charge transport and collection; and v) improve the stability of the active layer/electrode and, ultimately, the device. Perovskite solar cells use a variety of HTMs, including inorganic, polymer, and small organic molecules. Inorganic HTMs need thermal deposition, whereas solution-processable deposition destroys perovskite film, leading to a degraded absorption layer[2]. On the other hand, polymers have been associated with poor reproducibility due to batch to batch variance in polymerization or polydispersity. Another drawback of polymer HTMs is their low hole mobility, which their weak stacking would cause compared to small molecules. Molecules, on either hand, can be used as HTM to tackle repeatability difficulties since structural changes can easily change the purity, mobility, and optical properties [9].

To create smaller molecules that make good HTMs for perovskite solar cells, researchers must first investigate the structure-properties relationship, including the electronic structure of molecules as their constituents. Useful data about any molecule can be gathered by conducting a comprehensive theoretical and experimental study to understand bandgap, HOMO, and LUMO energy levels. This knowledge is crucial for understanding and designing appropriate compounds for solar cells. It has previously been reported that using DFT theory to predict geometry, electronic structure, and properties of conjugated materials is a good and trustworthy method [10, 11].

The present study focused on derivates of 1,3,5–tris (diphenylamino) benzene (TDAB) molecule. Scheme 1 depicts the design of novel 1,3,5–tris (diphenylamino) benzene (TDAB) derivatives. The computational investigation of various efficient small molecules-based HTMs in perovskite solar cells employing the DFT method with B3LYP/6-31G levels of theory is presented here. The systematic theoretical study sought a comprehensive knowledge of structure-property co-relationships and explored numerous optimal geometry properties such as bandgap, HOMO, and LUMO.

2. Computational Methodology

The structural, electronic, and optical properties of the studied hole transport materials HTM1-HTM9 have been explored using density functional theory (DFT) and time-dependent density functional theory (TD–DFT). S_0 and S_1 geometries of all HTMs were optimized using Beckethree–Lee–Yang–Parr (B3LYP) [12, 13]. For forecasting such geometries and attributes, functional analysis is effective [14–16]. The optimizations were carried out using the standard 6-31G basis set. [17–19] The polarizable continuum model (PCM) has been used to study the influence of acetonitrile (= 35.09) solvation. Gaussian 09W was used to calculate the geometries and electrical characteristics of neutral (ground and first excited states), cationic, and anionic forms, as well as reorganization energies [20]. Gauss View (version 5.0.8) [21] was used to do visual checks as part of this process. As a result, none of the HTM1-HTM9 geometries has imaginary frequencies, ensuring energy minima.

3. Result And Discussion

3.1 Geometry parameters- Dihedral angles

Six dihedral angles of the three connecting units to the central benzene ring were selected for the TDAB and HTM1-HTM9 at the ground state for gas and solvent optimization and are presented in Table 1. The optimized structures (Fig. 1) in the gas and solvent phase show that all molecules are non-planar with selected dihedral angles between 20^o and 50^o, and the non-planarity is due to the presence of sp^3 hybridized nitrogen a connecting atom [22]. Removal or addition of an electron from a molecule causes a noticeable effect on the value of dihedral angle as observed in the gas phase in Fig. 2, where the larger dihedral angle of anion optimized molecules for the angle C_1-C_6-N_7-$C_{12}$was observed compared to the dihedral angle of the cation indicating that much higher reorganization energy is required for the formation of anion from neutral molecule compared to the formation of cation from the neutral molecule. The TDAB and HTM1-HTM9 quickly form cation than anion molecule, thus efficiently transporting holes than an electron.

Table 1
The dihedral angles for TDAB and HTM1-HTM9 in gas and acetonitrile solvent.

S/NO	SELECTED DIHEDRAL ANGLES											
	Θ_1		Θ_2		Θ_3		Θ_4		Θ_5		Θ_6	
	gas	solvent	gas	solvent	gas	solvent	gas	solvent	gas	solvent	gas	solvent
TDAB	46.30	44.21	46.30	44.21	40.31	40.68	38.64	38.95	40.30	40.67	38.63	-38.94
HTM1	39.35	39.71	39.38	39.29	43.92	43.49	42.22	41.63	43.32	42.81	41.21	41.20
HTM2	48.74	44.85	48.61	45.27	40.28	41.57	38.70	39.89	39.19	41.71	38.11	39.98
HTM3	34.05	36.20	32.46	35.19	48.06	44.88	45.64	43.17	46.94	43.42	44.81	41.88
HTM4	40.42	40.07	40.69	39.80	44.14	43.66	42.10	41.83	41.31	40.66	39.69	39.20
HTM5	46.66	44.70	46.12	45.21	38.07	39.76	36.38	38.09	42.14	45.50	40.33	43.25
HTM6	35.22	35.97	34.67	34.54	48.69	46.48	47.16	44.52	40.53	36.08	39.73	35.96
HTM7	44.54	42.01	44.57	42.00	41.73	42.82	40.19	40.92	39.10	38.12	37.61	36.68
HTM8	42.77	42.88	42.85	43.15	38.54	40.08	36.74	38.31	50.33	50.31	48.11	48.32
HTM9	41.55	39.23	41.67	38.06	50.65	48.90	48.52	47.17	26.09	21.37	26.49	19.93

3.2. Ionization potential and electron affinity

According to the following equations[23], to determine the ionization potential and electron affinity using the DFT approach.

$IP = E_{cation} - E_{neutral}$ (1)

$EA = E_{anion} - E_{neutral}$ (2)

During the working of the perovskite solar cell, after an electron has been excited from the valence band of the perovskite active layer, an electron from the HOMO of the HTM has to drop and fill the hole left in the valence band of the perovskite; thus the ionization potential of the HTM has to be considerably lower to favour the process of electron transfer the HTM to the perovskite active layer, hence hole transfer from perovskite material to the HTM [24]. The lower the IP value, the easy formation of holes in the molecules under study; From Fig. 3 the lowest IP value was obtained by HTM 9; thus, tri addition of $-NH_2$ having a much contribution to the HOMO energy level has led to lower IP value[25].

3.3. Frontier molecular orbitals (HOMO-LUMO)

The HOMO and LUMO distributions and the energy levels of the structures examined are presented in Fig. 4 to help comprehend the electronic structure. In general, a good HOMO delocalization and an appropriate HOMO energy level relative to the valence band of perovskite are advantageous for improving the hole transfer integral and hole transport. The HOMO of the structures is estimated to be distributed over the entire molecule, whereas the LUMO is concentrated on the substitution core. It turns out that the HOMO is more broadly dispersed than the LUMO in the two derivatives, indicating that the derivatives have a good chance of being used as hole transport materials. Thus, energy and distribution of frontier molecular orbitals (FMOs) could be used to explain carrier transport features.

HOMO originated mainly from the entire molecule, while LUMO was primarily given by fragment A. As seen by the FMOs, HOMO delocalized approximately over the complete molecule for both molecules, while LUMO delocalized principally over fragment A for both. Hole transport is aided by the strengthening of the delocalization effect. There was also an increase in HTM/valence band overlaps between the HOMO of the TDAB as the HTM and the perovskite material, leading to enhanced charge extraction [24]. HTM9, which is produced by adding –NH2 to TDAB in tri addition, has the greatest HOMO level, as seen in Figure 2. Due to the existence of two lone pairs, HTM 2, HTM 5, and HTM 8 deviate from the increasing trend of HOMO energies due to increases and in the strength of the electron-donating group attached. HTM 8 has the lowest HOMO energy level of all the compounds under research and the spiro-OMeTAD, indicating a favorable overlap with the MAPbI3 perovskite active layer, according to the study.

3.4 Bandgap energy

The quantities of HOMO energy (EHOMO), LUMO energy (ELUMO), and their energy gap (H–L) were determined to understand the effect of the electrical characteristics better. Energy gaps represent the difference between HOMO and LUMO levels. The smaller the energy gap, the more likely the electronic transition [26–28], and the energy gap can be calculated using the following formula:

$$\Delta_{H-L} = |HOMO - LUMO|$$

1

The calculated HOMO, LUMO and Δ_{H-L} values TDAB and HTM1-HTM9 are listed in Table 2. The FMOs of TDAB and the designed HTM1-HTM9 must be compared to the MAPbI3 perovskite molecule shown in Fig. 5, which has HOMO energy of -5.44eV and LUMO energy of -4.0 eV, and the spiro-OMeTAD, which is currently in use and has HOMO energy of -5.07eV. The LUMO energy levels for the TDAB and HTM1-HTM9 were all above the LUMO energy level of the $MAPbI_3$ perovskite active layer and hence prevention of an electron excited from the valence band (VB) of the perovskite to the conduction band (CB) of the perovskite to fall in LUMO energy level of the HTM instead of the CB of the electron transport material.

Table 2
HOMO, LUMO and bandgap energy in eV for TDAB and HTM1-HTM9.

Molecules	GAS			ACETONITRILE		
	HOMO	LUMO	BAND GAP	HOMO	LUMO	BAND GAP
TDAB	-5.08	-0.77	4.30	-5.27	-0.97	4.30
HTM1	-5.02	-0.76	4.26	-5.23	-0.96	4.26
HTM2	-5.19	-0.88	4.31	-5.33	-1.03	4.31
HTM3	-4.81	-0.68	4.13	-5.01	-0.93	4.09
HTM4	-4.99	-0.73	4.26	-5.21	-0.94	4.27
HTM5	-5.28	-0.99	4.29	-5.35	-1.08	4.27
HTM6	-4.66	-0.53	4.13	-4.96	-0.86	4.09
HTM7	-4.95	-0.70	4.25	-5.17	-0.92	4.25
HTM8	-5.39	-1.12	4.27	-5.37	-1.12	4.25
HTM9	-4.40	-0.36	4.03	-4.79	-0.73	4.06

When the sun illuminates the PSC, electrons must be ejected from the perovskite active layer whose band energy gap is 2eV or less. For the HTM, the band energy gap has to be more than 2eV to avoid the parasitic loss of energy from the sun. The TDAB and HTM 1-9 show a band energy gap of between 4.0 to 4.3eV; thus, the low parasitic loss is expected to occur when used with the perovskite material. The solvent acetonitrile does not affect the band energy gap, as observed in Figure 6. On the other hand, HTM3, HTM6and HTM9, which mono, di, and tri substitution of $-NH_2$ respectively, were have lower values of band energy gaps. This has been due to the highest HOMO energy levels attained because the $-NH_2$ is the most influential electron-donating group among the selected groups and with a smaller bandgap, a redshift is expected to occur [29].

3.5 Charge transport properties

The reorganization energy ($\lambda_{h/e}$) refers to the energy change of the system, which is caused by the structural relaxation after the gain or loss of electrons. After a molecule has gained or lost an electron to form an anion or cation, the energy required for geometry modification is called reorganization energy. A change in dihedral angle gives a good prediction of a molecule's reorganization energy, but the reorganization energy of a molecule is inversely proportional to the charge mobility of the molecule. Thus lower reorganization energy of holes is a relevant factor for a hole transport material [30]. The reorganization energy is of two types: reorganization energy for the hole(λ_h) and electronic reorganization energy(λ_e). To optimize the anions and cations of the TDAB molecule and its derivatives to get the reorganization energies. The λ_h and λ_e energies calculated using the following equations[31–33]:

$$\lambda_h = (E_0^+ - E_+) + (E_+^0 - E_0)$$

2

$$\lambda_e = (E_0^- - E_-) + (E_-^0 - E_0)$$

3

Where $E_0^+ (E_0^-)$denotes the energy of cations (anions) resultant by optimizing the structure of neutral molecules. $E_+ (E_-)$ is the cation (anion) energy calculated using the optimized cation (anion) structure. $E_0^+ (E_0^-)$ is the neutral molecular energy determined in the cationic (anionic) state. E0 denotes the energy of the neutral molecule in its ground state. The calculated

reorganization energies of the hole for HTM1-HTM9 are present in Table 3 and show in Fig. 7. From the Table 3, the order of hole reorganization energies are as follows: HTM8 > HTM9 > HTM3 > HTM5 > HTM6 > HTM2 > HTM7 > TDAB ≈ HTM1 > HTM4.

Table 3
Charge transfer integral (V), Reorganization energies (λ), and charge transfer rate (K) for the TDAB and HTM1-HTM9.

molecule	λ_{holes} (eV)	$\lambda_{electrons}$ (eV)	λ_{Total} (eV)	V_{holes} (eV)	$V_{electrons}$ (eV)	$K_{(holes)}$ (s^{-1})	$K_{(electrons)}$ (s^{-1})
TDAB	0.170	0.315	0.484	0.022	0.017	3.93E+12	3.99E+11
HTM1	0.165	0.307	0.472	0.040	0.028	1.36E+13	1.17E+12
HTM2	0.252	0.340	0.592	0.005	0.004	6.18E+10	1.42E+10
HTM3	0.340	0.294	0.634	0.114	0.042	1.36E+13	3.07E+12
HTM4	0.159	0.309	0.468	0.032	0.020	9.42E+12	5.80E+11
HTM5	0.295	0.299	0.594	0.020	0.013	6.72E+11	2.67E+11
HTM6	0.274	0.297	0.571	0.051	0.028	5.83E+12	1.31E+12
HTM7	0.170	0.316	0.486	0.035	0.015	9.58E+12	2.96E+11
HTM8	0.469	0.333	0.802	0.051	0.011	6.57E+11	1.38E+11
HTM9	0.350	0.338	0.688	0.106	0.011	1.06E+13	1.21E+11

From Table 3, we can find that λ_{hole} of HTM4, HTM1 and HTM7 (0.159,0.165 and 0.170 eV, respectively) are smaller than other respective HTMs. Furthermore, it was observed that HTM 1, HTM 4 and HTM 7 with mono, di and tri substitutions of the $-CH_3$, respectively; this means that HTM4, HTM1 and HTM7 their hole transfer rate might be higher than other HTMs. Comparing λ_{hole} and λ_{elec} values of the four HTM4, HTM1, HTM2 and HTM7 indicate that the $\lambda_{hole} < \lambda_{elec}$. This also implies that the hole carrier mobility of such HTMs is greater than the electron carrier mobility. This means that these chemicals have the most significant hole-transporting potential.

3.6. Charge transfer rate (K)

It is widely known that reorganization energy (λ) no single parameter can explain the nature of charge transfer; consequently, we estimated the hole and electron transfer integrals and the intrinsic mobilities. The hole mobility of nine molecules was investigated using the Marcus theory. Marcus theory has been frequently used to determine the hole hopping rate (Kh) at room temperature, which may be stated as [34, 35]:

$$k_h = \frac{V^2}{\hbar}\left(\frac{\pi}{\lambda_h k_B T}\right)^{1/2} \exp\left(\frac{-\lambda_h}{4k_B T}\right)$$

4

V is the charge transfer integral, h is the reorganization energy, k_B is the Boltzmann constant, while T is the temperature (we usually use T = 300 K.) [36, 37]. According to the preceding equation, the hole hopping rate K_h is influenced by two crucial parameters: V and λ are broken into two parts: the electron transfer integral V_e and the hole transfer integral V_h [38]. The specific structure of molecular stacking is difficult [39–40], but the level-splitting approach gives good accessibility to face-to-face stacking [40], and this configuration can improve − coupling [41]. V_h is the hole transfer integral, and it can be calculated as follows [42–46]:

$$V_h = \frac{E_{HOMO} - E_{HOMO-1}}{2}$$

5

V_h is hole transport integral, E_{HOMO} and E_{HOMO-1} are the HOMO level and HOMO-1 level of face-to-face model HTMs dimer [40]. For a good HTM, the hole transfer rate must be more than the electron transfer rate in magnitude to ensure effective charge extraction and transfer to prevent electron and hole recombination. From Table 3 and Fig. 8, HTM 9, having the highest hole transfer rate compared to other molecules, is not suitable as HTM because of its higher magnitude of the electron transfer rate. Thus HTM6 showed the highest hole transfer rate of 1888.5 x 10^{-10} s^{-1} with a minimum magnitude of the electron transfer rate.

3.7 Absorption spectra

The absorption properties were characterized using the TD-DFT method with a 6-311G basis set on the ground state optimized structures in both gas and solvent (acetonitrile) to obtain information about the involved in the electronic transitions. The calculated maximum absorption wavelength (λ_{max})of TDAB and HTM1-HMT9 in the gas and solvent state are listed in Table 4.

Table 4
The ground state maximum absorption (λ_{max}) wavelength of TDAB and HTM1-HTM9 in gas and acetonitrile.

GAS PHASE					*SOLVENT PHASE*				
#	λmax	f	orbital contribution	% value	#	λmax	f	orbital contribution	% value
TDAB	337.47	0.0096	H-1 ->L+1	32.44	**TDAB**	346.31	0.0172	H-1 ->L+1	27.0539
			H ->L	64.11				H ->L	69.62
HTM1	339.12	0.0149	H-1 ->L+1	23.99	HTM1	348.25	0.0253	H-1 ->L+1	18.43581
			H ->L	72.01				H ->L	75.975
HTM2	337.54	0.003	H-1 ->L	6.42	HTM2	346.22	0.0084	H-1 ->L	37.81021
			H-1 ->L+1	37.49				H-1 ->L+1	5.233907
			H-1 ->L+2	2.03				H-1 ->L+2	2.262065
			H ->L	35.47				H ->L	18.87191
			H ->L+1	11.44				H ->L+1	30.78927
					HTM3	357.99	0.0377	H-1 ->L+1	4.929172
HTM3	344.77	0.0285	H-1 ->L+1	7.93				H ->L	85.60338
			H ->L	82.05				H ->L+1	3.401875
HTM4	339.21	0.0108	H-1 ->L	2.39	HTM4	348.29	0.0176	H-1 ->L	6.48216
			H-1 ->L+1	26.27				H-1 ->L+1	18.87191
			H ->L	65.05				H ->L	63.35102
			H ->L+1	2.80				H ->L+1	7.846345
HTM5	337.79	0.0076	H-1 ->L	15.69	HTM5	346.48	0.0184	H-1 ->L	28.48011
			H-1 ->L+1	24.49				H-1 ->L+1	7.790194
			H ->L	41.03				H ->L	33.2977
			H ->L+1	11.25				H ->L+1	24.44403
			H ->L+3	2.18	HTM6	354.85	0.0087	H-2 ->L	2.128397
HTM6	344.09	0.006	H-1 ->L	28.42				H-1 ->L	30.96845
			H ->L	13.38				H ->L	16.57843
			H ->L+1	51.71				H ->L+1	45.42189
HTM7	226.63	0.0019	H-2 ->L+8	3.44	HTM7	349.1	0.0165	H-1 ->L	11.045
			H-2 ->L+11	2.52				H-1 ->L+1	16.00422
			H-1 ->L+1	14.96				H ->L	55.93223
			H-1 ->L+6	8.61				H ->L+1	13.37583
			H-1 ->L+9	3.47	HTM8	346.95	0.0226	H-1 ->L	19.90679
			H ->L+2	14.58				H-1 ->L+1	3.794462
			H ->L+3	5.61				H ->L	27.91689

GAS PHASE					*SOLVENT PHASE*				
			H ->L+7	6.18				H ->L+1	41.68575
			H ->L+10	3.71	HTM9	358.64	0.0184	H-1 ->L+1	5.763013
HTM8	355.67	0.0099	H-1 ->L+1	23.39				H ->L	65.00052
			H ->L	70.78				H ->L+1	22.36066
HTM9	351.69	0.0151	H-1 ->L+1	6.16					
			H ->L	88.22					

The absorption spectrum of each HTM is represented in Fig. 9&10, the absorption of TDAB and HTM1-HMT9 in the gas phase was observed to occur within the UV region; thus, no absorption occurred in the visible region that will cause a parasitic loss due to decreased amount of energy from the sun to cause the excitation in the perovskite active layer. Instead, all the energy from the sun in the visible region of the spectrum will cause electron transitions in the perovskite active layer. Thus the TDAB and HTM1-HMT9 are transparent in the visible region of the spectrum in gas-phase calculations, with HTM 7 having the lowest value of λ_{max}. A redshift was also observed in solvent phase calculations, and this can be explained by the use of high dielectric constant solvent, acetonitrile, which contributes to the electron density, causing a decrease in the band gap.

4. Conclusions

DFT and TD–DFT methods have been used to investigate the studied HTM molecules for structural, electronic and optical properties. Six dihedral angles of the three connecting units to the central benzene ring were selected for the TDAB and HTM 1-9 show that all molecules are non-planarity. The FMOs of TDAB and the designed HTM 1-9 must be compared to the MAPbI3 perovskite molecule and all of the compounds under investigation, and the spiro-OMeTAD, HTM 8 has the lowest HOMO energy level, indicating a favourable overlap with the MAPbI3 perovskite active layer. The TDAB and HTM 1-9 show a band energy gap of between 4.0 to 4.3eV; thus, the low parasitic loss is expected to occur when used with the perovskite material. On the other hand, HTM 3, HTM 6and HTM 9, which mono, di, and tri substitution of $-NH_2$ respectively, were honoured to have lower values of band energy gaps. From UV absorption calculations, the TDAB and HTM 1-9 are transparent in the visible spectrum region in gas-phase calculations, with HTM 7 having the lowest value of λ_{max}. The reorganization energy of holes and electrons was calculated, and it was observed that HTM 1, HTM 4 and HTM 7 with mono, di and tri addition of the $-CH_{3,}$ respectively and HTM 9, having the highest hole transfer rate compared to other molecules.

References

1. Yang WS, Park BW, Jung EH et al.. Iodide management in formamidinium-lead-halide-based perovskite layers for efficient solar cells. *Science*. 2017;356(6345):1376-1379.
2. Park NG, Grätzel M, Miyasaka T, et al.Towards stable and commercially available perovskite solar cells. *Nat Energy*. 2016;1(11):16152.
3. Han Q, Hsieh YT, Meng L et al.. High-performance perovskite/Cu(In,Ga)Se2 monolithic tandem solar cells. *Science*. 2018;361(6405):904-908.
4. National Renewable Energy Laboratory. Best research-cell efficiency chart, NREL. https://www.nrel.gov/pv/cell-efficiency.html; 2019.
5. Kou C, Feng S, Li H et al.. Molecular “Flower” as the High-Mobility Hole-Transport Material for Perovskite Solar Cells. *ACS Appl Mater Interfaces*. 2017;9(50):43855-43860.
6. Sun Z-ZZ, Xu Y-LL, Zhu R, Liu H-YY. How to stabilize the HOMO levels and to improve the charge transport properties of hole-transporting materials? Probing the effects of molecular symmetry. *Org Electron*. 2018;63:86-92.
7. Maciejczyk M, Ivaturi A, Robertson N. *J Mater Chem A*. 2016;4:1-22.

8. Calió L, Kazim S, Grätzel M, Ahmad S. Hole-transport materials for perovskite solar cells. *Angew Chem Int Ed Engl*. 2016;55(47):14522-14545.
9. Shahjad R, Bhargav D, Bhardwaj A. Patra, Electronic levels of small molecules for organic solar cells: a computational study, Advanced Materials. *Proceedings*. 2017;2(5):294-298.
10. Zade SS, Bendikov M. From oligomers to Polymer: convergence in the HOMO– LUMO gaps of conjugated oligomers. *Org Lett*. 2006;8(23):5243-5246.
11. Zade SS, Zamoshchik N, Bendikov M. From short conjugated oligomers to conjugated polymers. Lessons from studies on long conjugated oligomers. *Acc Chem Res*. 2011;44(1):14-24.
12. Becke AD. Density-functional exchange-energy approximation with correct asymptotic behavior. *Phys Rev A Gen Phys*. 1988;38(6):3098-3100.
13. Lee C, Yang W, Parr RG. Development of the Colle-Salvetti correlation-energy formula into a functional of the electron density. *Phys Rev B Condens Matter*. 1988;37(2):785-789.
14. Chi WJ, Li ZS. The theoretical investigation on the 4-(4-phenyl-4-α-naphthylbutadieny)-triphenylamine derivatives as hole transporting materials for perovskite-type solar cells. *Phys Chem Chem Phys*. 2015;17(8):5991-5998.
15. Chen X, Jia C, Wan Z, Zhang J, Yao X. Theoretical investigation of phenothiazine–triphenylamine-based organic dyes with different π spacers for dye-sensitized solar cells. *Spectrochim Acta A Mol Biomol Spectrosc*. 2014;123:282-289.
16. Bagheri Novir S, Hashemianzadeh SM. Density functional theory study of new azo dyes with different π-spacers for dye-sensitized solar cells. *Spectrochim Acta A Mol Biomol Spectrosc*. 2015;143:20-34.
17. Tomasi J, Mennucci B, Cammi R. Quantum mechanical continuum solvation models. *Chem Rev*. 2005;105(8):2999-3093.
18. Cossi M, Barone V. Time-dependent density functional theory for molecules in liquid solutions. *J Chem Phys*. 2001;115(10):4708-4717.
19. Adamo C, Barone V. A TDDFT study of the electronic spectrum of s-tetrazine in the gas-phase and in aqueous solution. *Chem Phys Lett*. 2000;330(1-2):152-160.
20. Frisch MJ, Trucks GW, Schlegel HB et al. Gaussian. 2016;09. Revision A.02 Edition. Gaussian, Inc., Wallingford C.
21. Roy Dennington K, T, Millam J; 2009. *GaussView*. version 5 Edition Mission S, ed. KS: Semichem Inc.
22. McKelvey RD. Stereochemistry of organic compounds (Eliel, Ernest L.; Wilen, Samuel H.). *J Chem Educ*. 1996;73(8):A174.
23. Chitpakdee C, Namuangruk S, Khongpracha P et al. Theoretical studies on electronic structures and photophysical properties of anthracene derivatives as hole-transporting materials for OLEDs. *Spectrochim Acta A Mol Biomol Spectrosc*. 2014;125:36-45.
24. Naqvi S, Patra A. Hole transport materials for perovskite solar cells: A computational study. *Mater Chem Phys*. 2021;258, PubMed: 123863.
25. Wazzan N, El-Shishtawy RM, Irfan A. DFT and TD–DFT calculations of the electronic structures and photophysical properties of newly designed pyrene-core arylamine derivatives as hole-transporting materials for perovskite solar cells. *Theor Chem Acc*. 2018;137(1).
26. Sahli F, Werner J, Kamino BA et al.. Fully textured monolithic perovskite/silicon tandem solar cells with 25.2% power conversion efficiency. *Nat Mater*. 2018;17(9):820-826.
27. Chiba T, Hoshi K, Pu YJ et al.. High-Efficiency Perovskite Quantum-Dot Light-Emitting Devices by Effective Washing Process and Interfacial Energy Level Alignment. *ACS Appl Mater Interfaces*. 2017;9(21):18054-18060.
28. Frost JM, Butler KT, Brivio F, Hendon CH, van Schilfgaarde M, Walsh A. Atomistic origins of high-performance in hybrid halide perovskite solar cells. *Nano Lett*. 2014;14(5):2584-2590.
29. *Materials*, Qiu DHT, M, Pei W et al. 2019. *applied sciences DFT Characteristics of Charge Transport in*:1-7.
30. Ashassi-Sorkhabi H, Salehi-Abar P. How the change of OMe substituent position affects the performance of spiro-OMeTAD in neutral and oxidized forms: theoretical approaches. *RSC Adv*. 2018;8(33):18234-18242.
31. Shi XL, Yang YH, Wang LH, Li Y. Introducing Asymmetry Induced by Benzene Substitution in a Rigid Fused π Spacer of D−π−A-Type Solar Cells: A Computational Investigation. *J Phys Chem C*. 2019;123(7):4007-4021.

32. Christians JA, Fung RCM, Kamat PV. An inorganic hole conductor for organo-lead halide perovskite solar cells. Improved hole conductivity with copper iodide. *J Am Chem Soc*. 2014;136(2):758-764.
33. Sha WEI, Zhang H, Wang ZS et al. *Adv Energy Mater*. 2018;8:7.
34. Irfan A, Assiri M, Al-Sehemi AG. Exploring the optoelectronic and charge transfer performance of diaza[5]helicenes at molecular and bulk level. *Org Electron*. 2018;57:211-220.
35. Zhang Y, Li Y, Chen C, Wang L, Zhang J. Design new hole transport materials for efficient perovskite solar cells by suitable combination of donor and core groups. *Org Electron*. 2017;49:255-261.
36. Lan YK, Huang CI. A theoretical study of the charge transfer behavior of the highly regioregular poly-3-hexylthiophene in the ordered state. *J Phys Chem B*. 2008;112(47):14857-14862.
37. Marcus RA. Chemical and Electrochemical Electron-Transfer Theory. *Annu Rev Phys Chem*. 1964;15(1):155-196.
38. Gapol MAB, Balanay MP, Kim DH. Molecular Engineering of Tetraphenylbenzidine-Based Hole Transport Material for Perovskite Solar Cell. *J Phys Chem A*. 2017;121(6):1371-1380.
39. Ashassi-Sorkhabi H, Salehi-Abar P, Asghari E, Kazempour A. Structural effect on the thermodynamic and electrochemical properties of pyrene-based hole transport materials. *J Mol Liq*. 2019;285:338-346.
40. Kirkpatrick J, Nelson J. Theoretical study of the transfer integral and density of states in spiro-linked triphenylamine derivatives. *J Chem Phys*. 2005;123(8):084703.
41. Valeev EF, Coropceanu V, da Silva Filho DA, Salman S, Brédas JL. Effect of electronic polarization on charge-transport parameters in molecular organic semiconductors. *J Am Chem Soc*. 2006;128(30):9882-9886.
42. Xu YL, Ding WL, Sun ZZ. How to design more efficient hole-transporting materials for perovskite solar cells? Rational tailoring of the triphenylamine-based electron donor. *Nanoscale*. 2018;10(43):20329-20338.
43. Berlin YA, Hutchison GR, Rempala P, Ratner MA, Michl J. Charge Hopping in Molecular Wires as a Sequence of Electron-Transfer Reactions. *J Phys Chem A*. 2003;107(19):3970-3980.
44. Brédas JL, Calbert JP, da Silva Filho DA, Cornil J. Organic semiconductors: a theoretical characterization of the basic parameters governing charge transport. *Proc Natl Acad Sci U S A*. 2002;99(9):5804-5809.
45. Li M, Li N, Chen G et al.. Perovskite solar cells based on chlorophyll hole transporters: dependence of aggregation and photovoltaic performance on aliphatic chains at C17-propionate residue. *Dyes Pigm*. 2019;162:763-770.
46. Zhang Y, Guo J, Su H, Li J, Wu W, Wang L. A rational design of hole-transport small molecules based on fluorene with different modified groups for organic lead-halide perovskite solar cells. *Dyes Pigm*. 2018;154:275-281.

Scheme

Scheme 1 is available in supplementary section

Figures

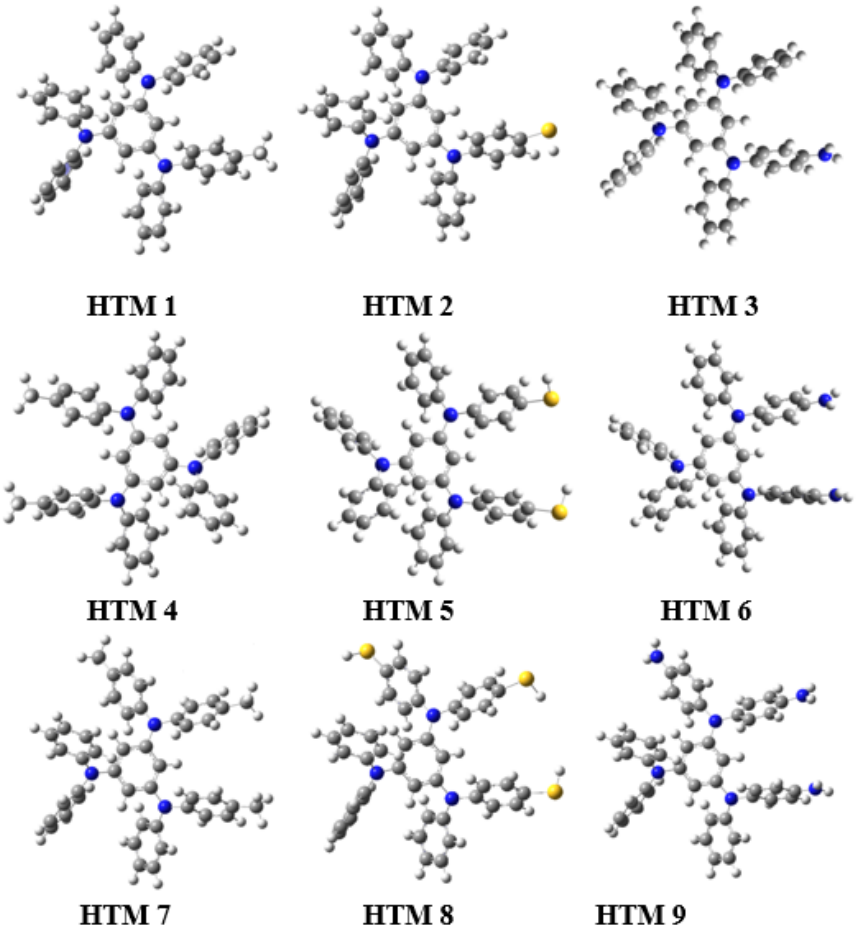

Figure 1

Optimized structures of the TDAB and HTM 1-9 in gas phase by using DFT/B3LYP method with 6-311G basis set.

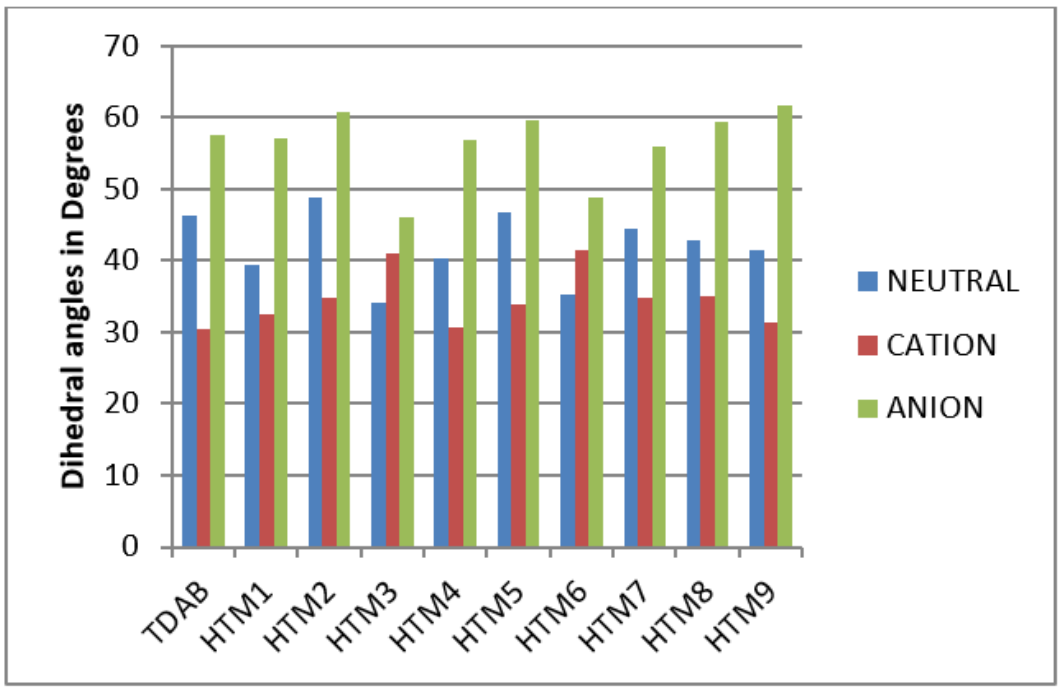

Figure 2

The dihedral angles of neutral, cation, and anion optimized structures of TDAB and HTM 1-9 in the gas phase.

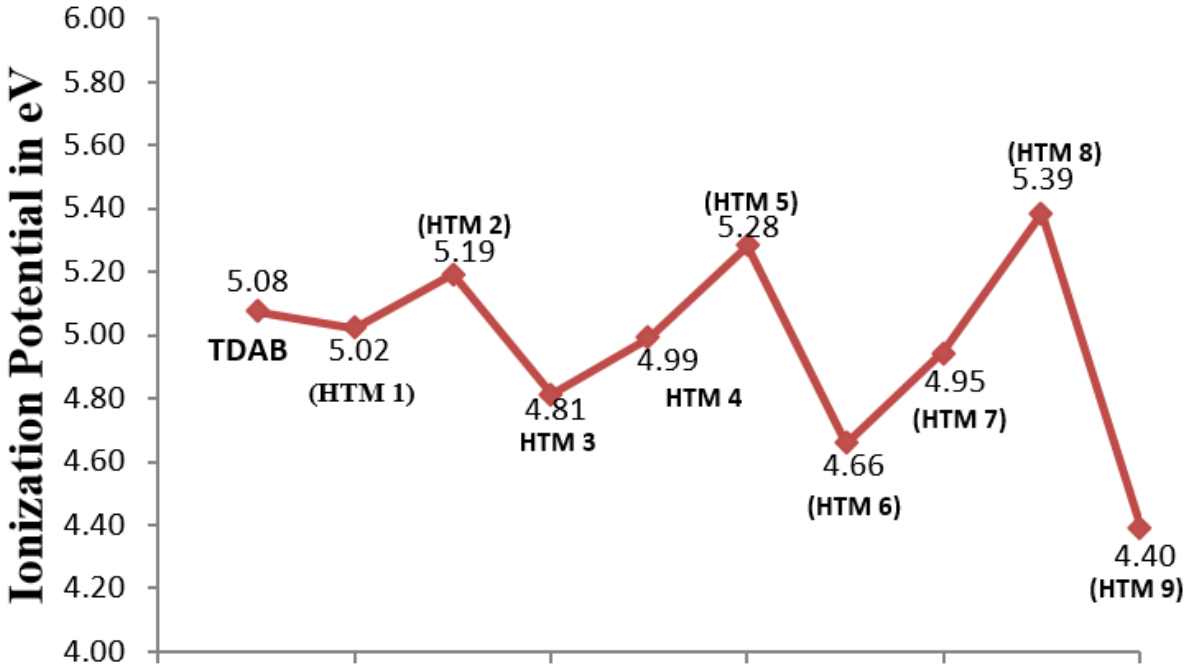

Figure 3

Ionization potentials of TDAB and HTM 1-9 in gas phase by using DFT/B3LYP method with 6-311G basis set.

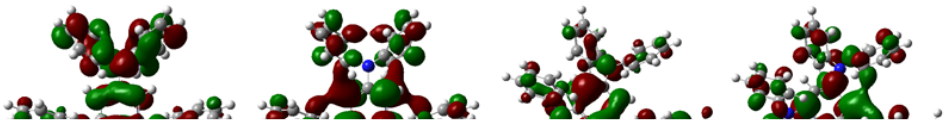

Figure 4

HOMO and LUMO surface plots of the TDAB and HTM 1-9 in gas phase by using DFT/B3LYP method with 6-311G basis set.

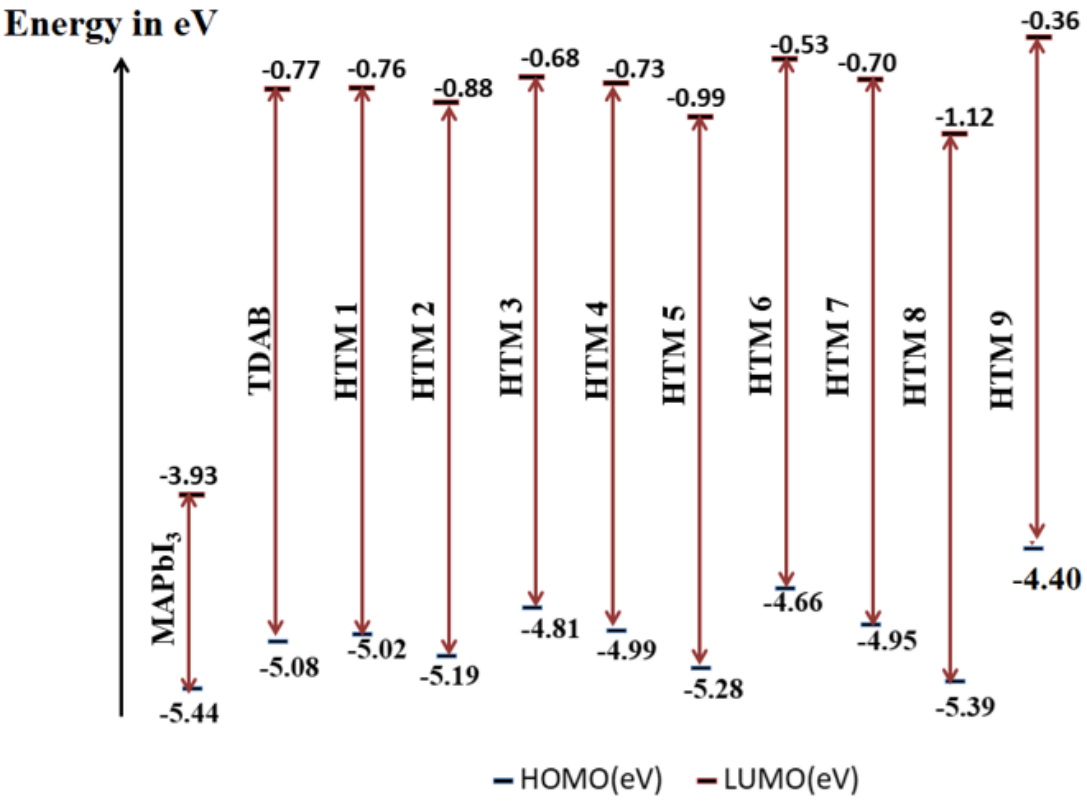

Figure 5

HOMO and LUMO energy level diagram of TDAB and HTM 1-9 in the gas phase.

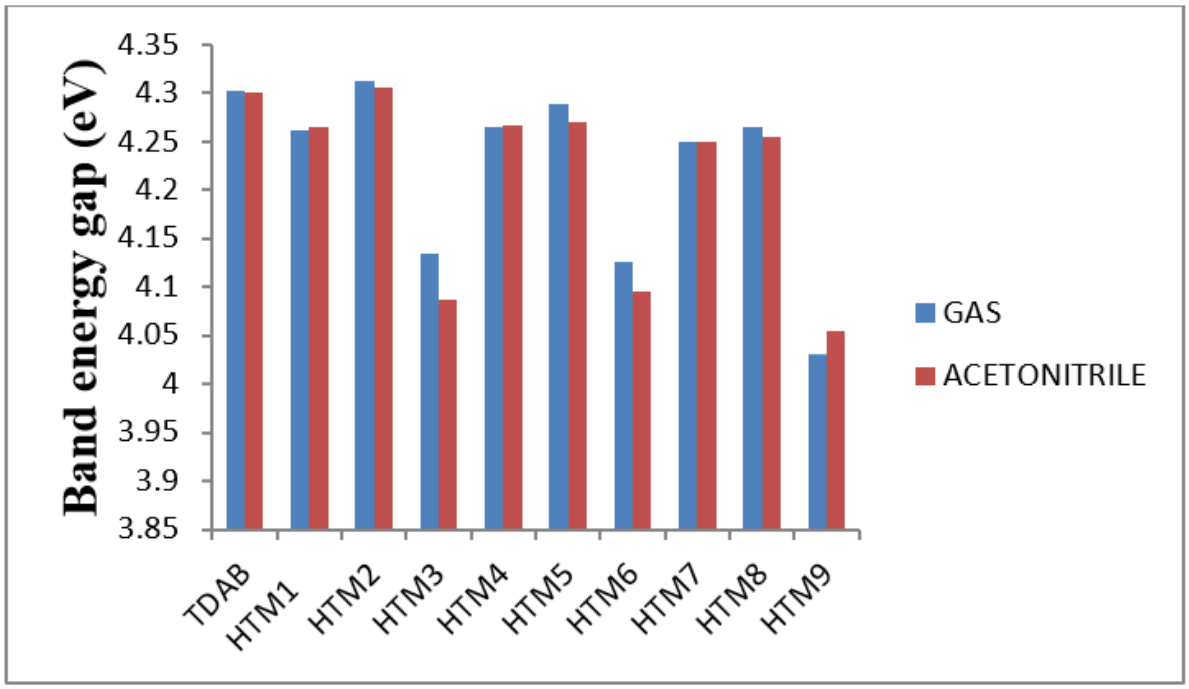

Figure 6

Band energy gaps for TDAB and HTM 1-9 in gas and acetonitrile solvent by using DFT/B3LYP method with 6-311G basis set.

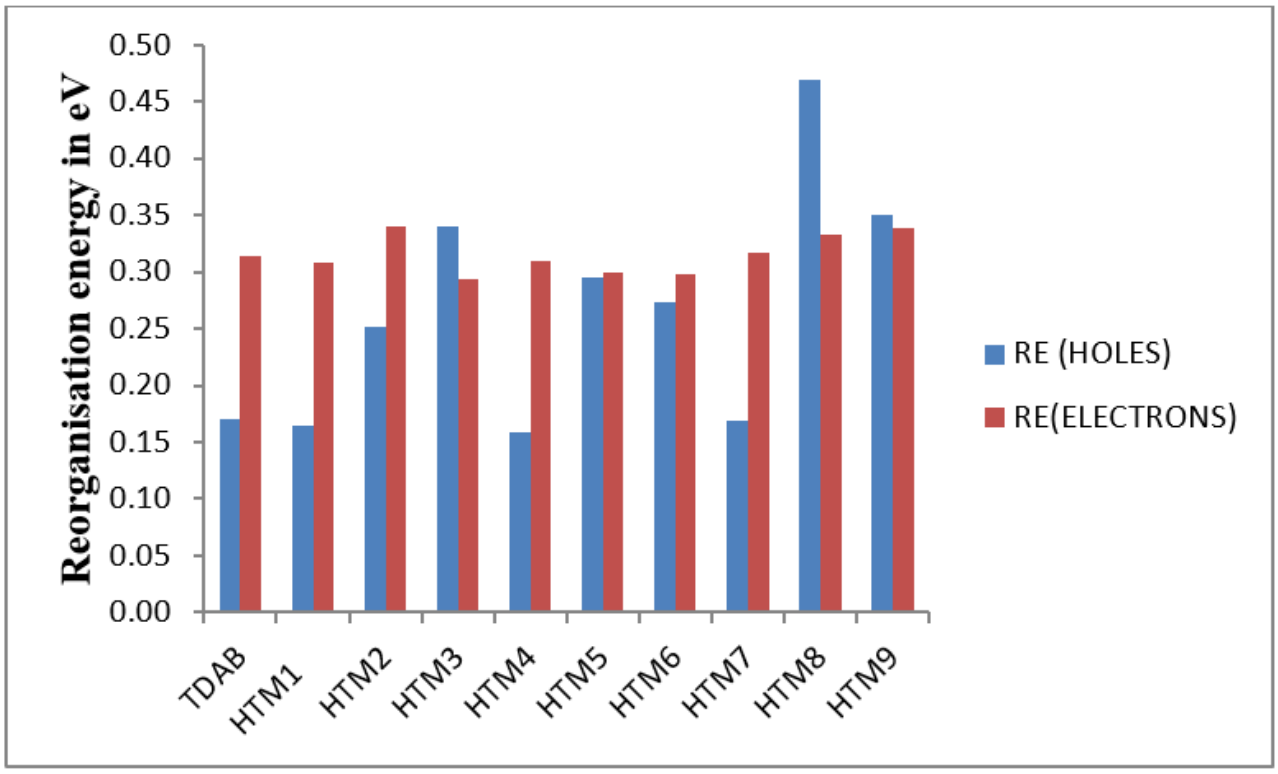

Figure 7

Reorganization energy of holes and electrons for TDAB and HTM 1-9 in gas phase by using DFT/B3LYP method with 6-311G basis set.

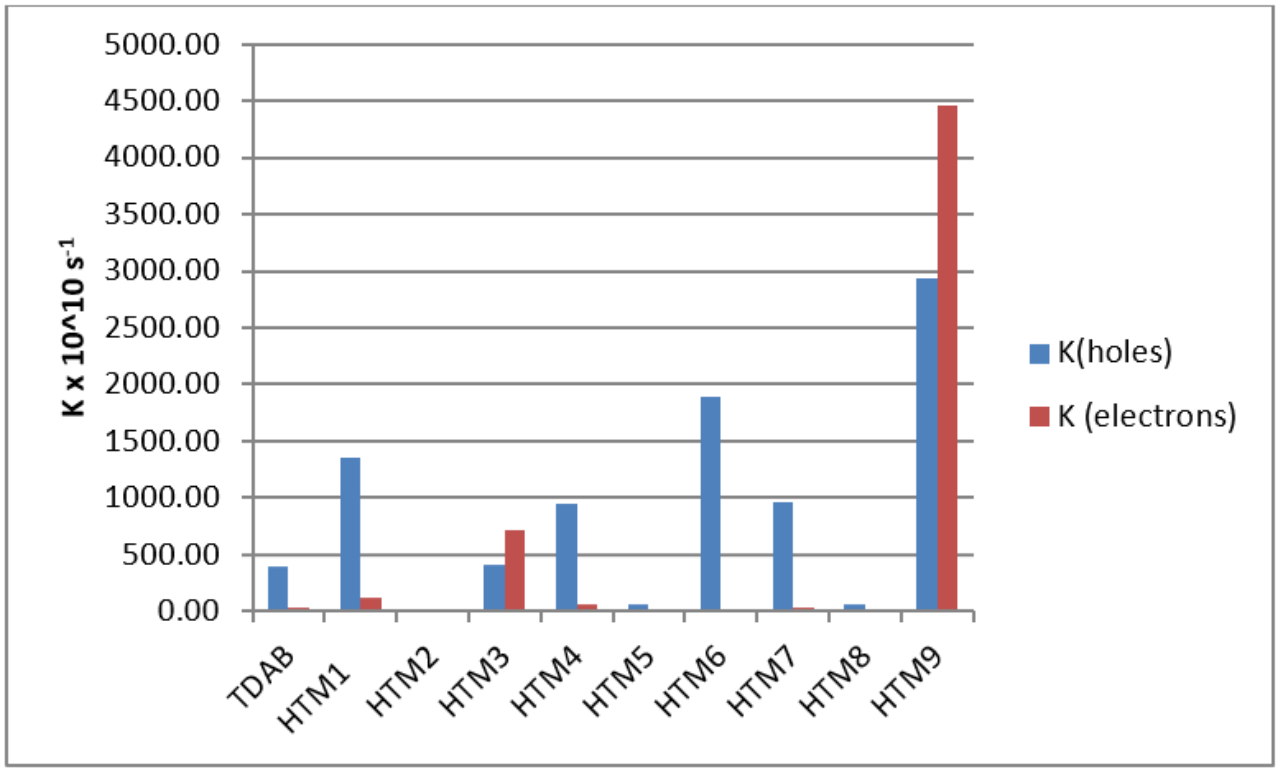

Figure 8

Charge transport rate diagram for holes and electrons of TDAB and HTM 1-9 in the gas by using TD-DFT/B3LYP method with 6-311G basis set.

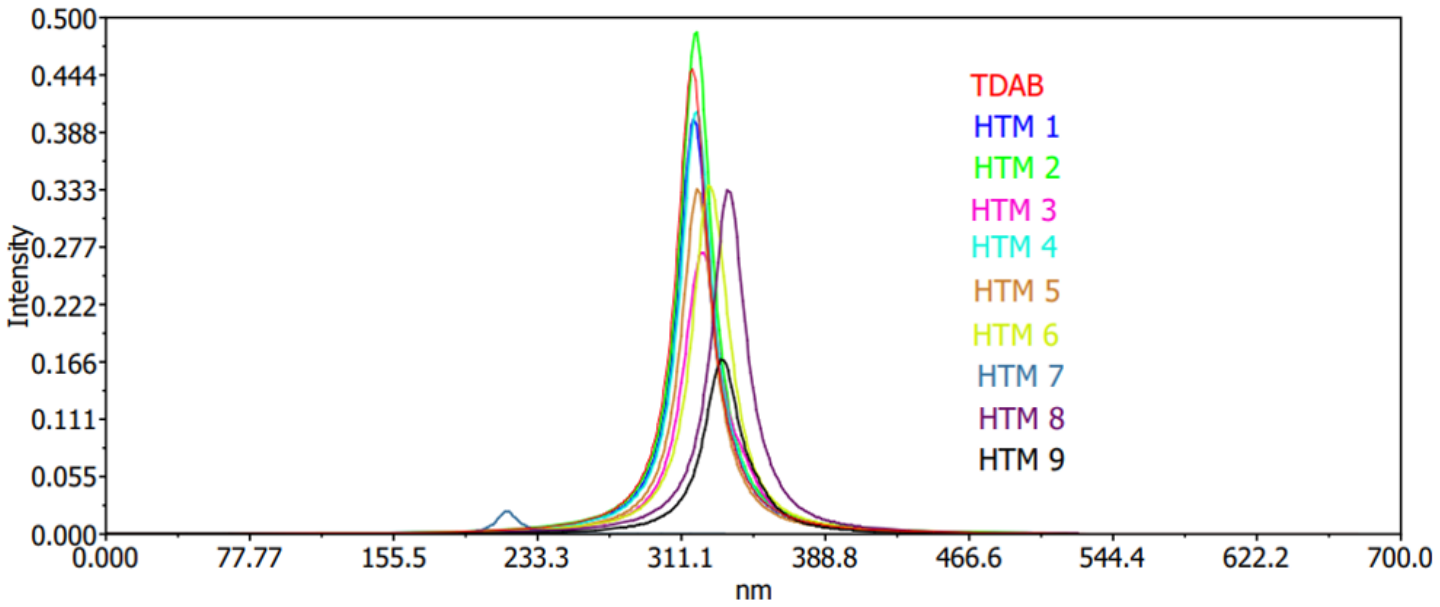

Figure 9

Charge transport rate diagram for holes and electrons of TDAB and HTM 1-9 in the gas by using TD-DFT/B3LYP method with 6-311G basis set.

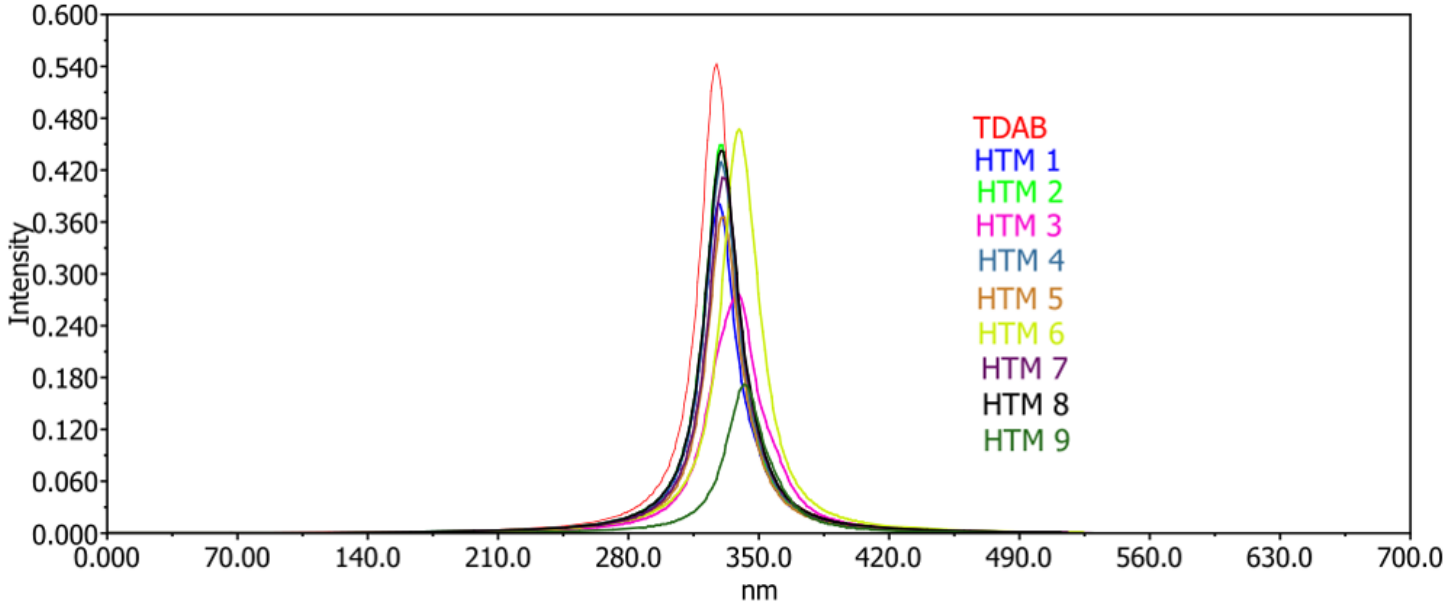

Figure 10

Charge transport rate diagram for holes and electrons of TDAB and HTM 1-9 in the solvent by using TD-DFT/B3LYP method with 6-311G basis set.

Supplementary Files

This is a list of supplementary files associated with this preprint. Click to download.

- scheme1.png